**Article**

# Exploding the Dark Heart of Chaos: Part I

**Chris King***

Mathematics Department, University of Auckland

## ABSTRACT

This paper, with its associated graphical software and movies, is an investigation of the universality of the cardioid at the centre of the cyclone of chaotic discrete dynamics, the quadratic 'heart' forming the main body of the classic Mandelbrot set. Using techniques investigating and exploring the continuity, bifurcations and explosions in its related Julia sets, we demonstrate its universality across a wide spread of analytic functions of a complex variable, extending from the classical quadratic, through higher polynomials and rational functions, to transcendental functions and their compositions. The approach leads to some interesting and provocative results, including decoding dendritic island periodicities, and multiple critical point analysis, leading to layered Mandelbrot set 'parameter planes', and intriguing issues of critical point sensitivity in the irregular structures in the Mariana trenches of the more complex functions. Part I of this article includes: 1. Real 'Boom and Bust' Origins of the Dark Heart; 2. Illuminating the Writhing Dark Heart of Complexity; 3. The Dark Heart's Magic Numerology; and 4. A Heart is only Half a Hamburger: Degenerate Critical Points.

**Key Words:** chaos, cardioid, cyclone, Mandelbrot set, Julia set, bifurcation, analytic function.

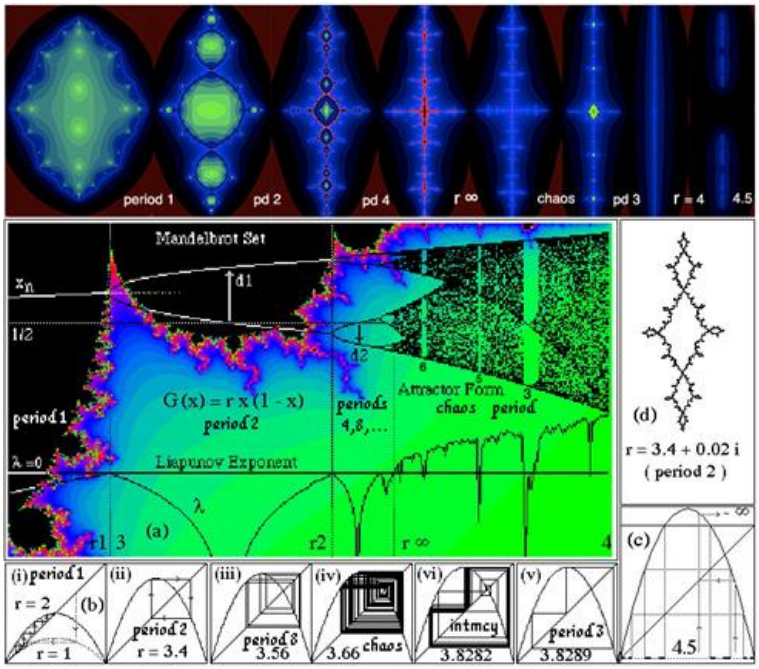


Fig 1: Manifestation of chaos in population boom and bust. Centre: the bifurcation diagram with the bulbs of the corresponding Mandelbrot set, showing identical periodicities. Top row: Corresponding Julia sets as boundary between inner and outer basins highlighted by their level sets. Right Period 2 Julia set by modified inverse iteration. Bottom row. Dynamics by iterating $y = f(x)$ and $x = y$. At 4.5 the domain fragments into a fractal Cantor set.

* Correspondence: Chris King http://www.dhushara.com E-Mail: chris@sexualparadox.org
Note: This work was completed 8th March – 22nd April 2009.

### 1. Real 'Boom and Bust' Origins of the Dark Heart

To understand the basis of the black heart in complex numbers it is useful to start with a straightforward process in real numbers, which is also at the heart of both chaos theory and world futures – population boom and bust. Suppose we have a population that breeds each spring according to exponential natural growth, so that the next season's population $x_n$ would be $x_{n+1} = rx_n$. If we also limit the growth to be proportional to the remaining food area $1 - x_n$, we end up with the so-called logistic iteration $x_{n+1} = G(x_n) = rx_n(1 - x_n)$ [1.1].

We can follow this process graphically, by first calculating $y = G(x)$ and then letting $x = y$, as shown in the various small graphs in fig 1(b). As the parameter *r* varies upwards from 1, a whole series of changes occur in the dynamics at discrete values called bifurcation points. Firstly the population reaches equilibrium – a fixed point where $G(x) = x$, then at $r = 3$ we suddenly find a good year and a lean year – the birth of a period 2 attractor, followed by an infinite sequence of period doublings 4, 8, 16, 32 etc. until in the limit at $r^{\infty}$, we get our first sight of classical chaos – the iteration, although deterministic, appears to wander over the domain in a seemingly random manner. If we plot the limit points the iteration ends up in, for increasing values of *r*, we get the Feigenbaum bifurcation diagram of attractor form, with the repeated pitchforks and dappled chaotic fan in fig 1(a). The third prong of the pitchfork is the old period 1 fixed point attractor, which has now become repelling towards the new period 2 attractor, as shown dotted in the first fork.

We can tell we are in chaos, because the process displays the 'butterfly effect', coined by Edward Lorenz – that if the weather is chaotic, the subtle disturbance of a butterfly flying in the botanical gardens in Hawaii could become the seed of a tropical cyclone hitting Fiji – otherwise known as *sensitivity on initial conditions* – that arbitrarily small initial differences can lead to global divergences. We can even plot the average rate of exponential spreading, using the Lyapunov exponent, which is positive in chaos, but plunges negatively towards $-\infty$ as the ordered periodicities move from attracting to super-attracting fig 1(a).

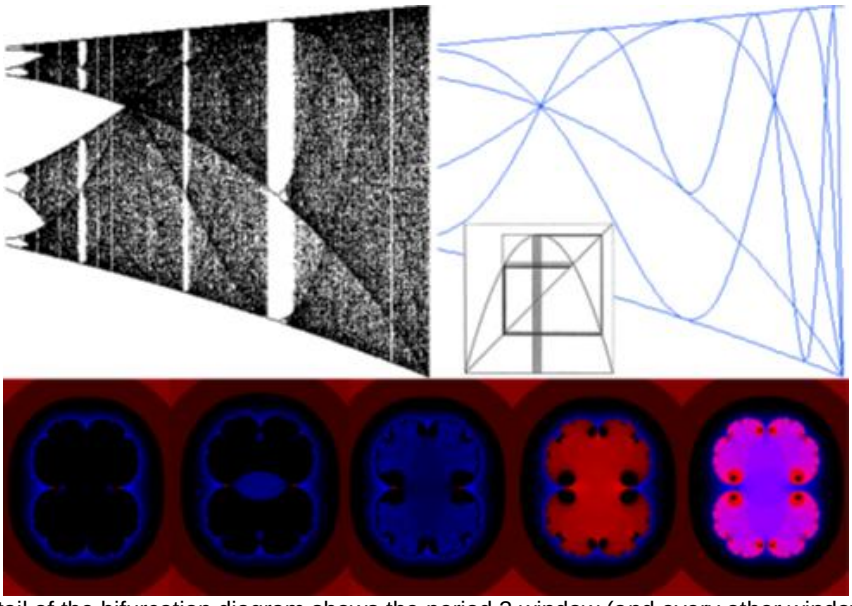

Fig 2: Above: Detail of the bifurcation diagram shows the period 3 window (and every other window) has on the left an abrupt transition from chaos by intermittency crisis and on the right a period doubling sequence (3, 6, 9 …). The importance of the critical points is shown by plotting successive graphs of iterates $f_n(r) = G_r^{(n+1)}(1/2)$ of the critical value with varying *r,* which correspond to the darkened curves in the chaotic region because orbits are drawn together there (inset). Below: The explosion of the complex Julia set from a closed curve to disconnected Cantor dust

at a single point, as we exit the right hand cusp of the cardioid of fig 3 shows intermittency crisis at work in the complex case.

In the midst of chaos there are also a series of windows of other periods. In the centre right is a period 3 window, followed to the left by a sequence of all odd periods 3, 5, 7 etc and then, in a reflected series of period doublings, series of even multiples 6, 10, 14 etc. These fall into a number sequence determined by Sarkovskii's theorem, which applies to all continuous real functions: Attracting periods further to the right in the following series of all natural numbers have hidden periodicities of all the values to the left:

$$1 > 2 > 4 > \mathrm{K} > 2^n > \mathrm{K}\ 2^n \cdot odd \mathrm{K} > \mathrm{K}\ 2.odd \mathrm{K}\ 7 > 5 > 3 \quad [1.2].$$

Each window has an abrupt transition from chaos to order, followed as it closes by an infinite period doubling sequence into chaos again. Finally we see our first sign of fractals fig 1(c). When we go past $r = 4$, the process becomes unstable, because a central interval of points escapes [0,1] in the first step and tends to $-\infty$, and the two smaller remaining intervals each have a sub-interval escaping 2 steps, and so on, so that, in the limit, we are left with a totally disconnected residual fractal, called a Cantor set, which has an endlessly repeating motif of self-similarity, in which any part has the same recursive structure as the whole, in the manner of a snowflake.

The question naturally arises: Why are we getting so many different dynamical answers here? Why so many systems doing apparently different things? Is there no natural unification at all, in this mix of order and chaos? This is where the beauty of complex numbers enters into the picture.

In the top row of fig 1 are the corresponding chaotic Julia sets of the same complex number iteration, with their x-coordinates vertical. For period 1 the Julia set intersects the real line transversely at only two points, one repelling fixed point and the point which reflects into it, leaving all the other real points attracted to the attracting fixed point in an ordered manner. By contrast for $r$ = 4, the Julia set has become an interval lying directly along the x-axis, resulting in real chaos on the number line.

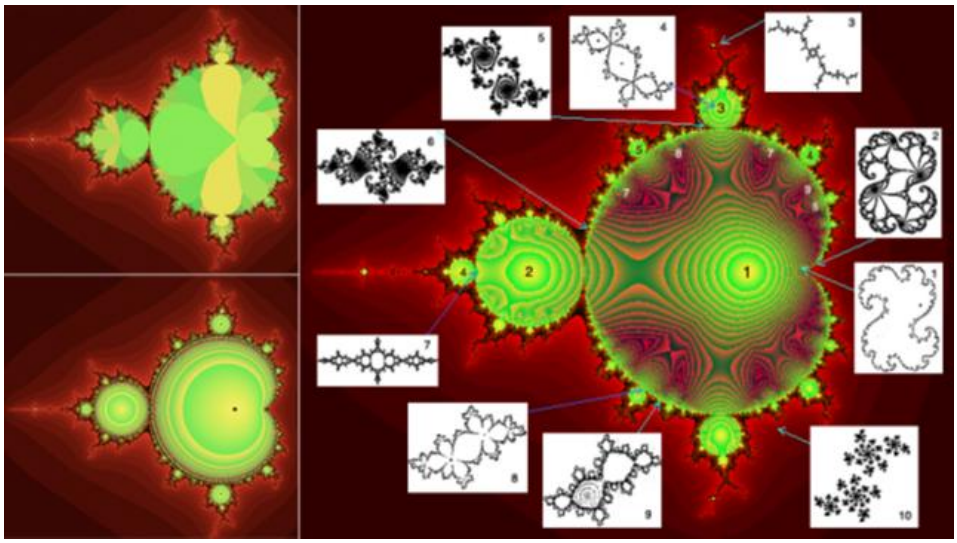

Fig 3: Lightening up the dark heart of the Mandelbrot set of $f(z) = z^2 + c$: (Right) illuminating the closest approach the iterates of the origin (critical point) make to the origin inside the set, as well as its exterior level sets, surrounded by some of its associated Julia sets plotted by modified inverse iteration (see below). (Top left) Partitioning into which iterate of the critical point makes the closest approach. (Bottom left) Internal level sets of periodic attractors.

## 2. Illuminating the Writhing Dark Heart of Complexity

If we iterate using the plane of complex numbers, instead of the real number line, we find that every possible $r$ value has a fractal set of points on which it is chaotic, called the Julia set, surrounded by one or

more ordered basins tending to fixed and periodic points, as shown in fig 3, for the quadratic function

$$f(z) = z^2 + c \quad [2.1].$$

The Mandelbrot set forms an atlas, or 'parameter plane' of the Julia sets plotted by the level set method, which we will explain below. Inverse iteration turns the repelling Julia set into an attractor by solving $z_n = \pm\sqrt{z_{n+1} - c}$ [2.2] repeatedly, starting from a repelling fixed point $f(z) = z^2 + c = z$, (there is always at least one) to get $2^{n+1}$ points on $J_c$. It can be further refined by focusing on points that are weakly attracting, using the derivative to eliminate repeated and strongly attracting iterates. This helps get around the fact that despite a Julia set being repelling overall, there are exponential variations in probability density of the iteration, which causes the inverse process to fail to represent weakly attracting areas, no matter how long the iterative method runs.

Now we get to the topological nub of the problem! Some Julia sets are connected as in 1 and 4 in fig 3, and have internal basins tending to a period 1 and 3 attractor respectively shown as dots. However others are totally disconnected Cantor sets – 2D versions of the one we saw in fig1(c), illustrated by 5 and 10. Continuity of the Julia sets is the question that led to the discovery of the Mandelbrot set as the atlas set of $c$ values for which the Julia set is connected, as shown in fig 3. At first sight, it is far from obvious how one could possibly characterize the set of points for which a complex 2-dimensional fractal will be topologically connected, and it took from Julia in the 1920s to Mandelbrot in the 1980s for the full fractal nature of the black heart to become apparent, instigated by an ASCII image in *'s the actual discoverer sent to him.

We can derive the central period 1 cardioid of this set fairly easily. For obvious reasons to do with net shrinkage of neighbouring points to the attractor, it turns out that a periodic attractor has absolute derivative $|f'(z)| < 1$ [2.3], so if we look for the boundary of where we have period 1 – i.e. $f(z) = z^2 + c = z$, with $|f'(z)| = 1$ [2.4], and solve for $c$ in terms of $z$, where $f'(z) = 2z = e^{i\theta}$ we get $c = z - z^2 = \frac{e^{i\theta}}{2} - \frac{e^{2i\theta}}{4}$ [2.5], the equation for the cardioid. We can also immediately see that the positions of the bases of the period-$q$ bulbs will correspond to $f'(z) = e^{2\pi ip/q}$, giving their positions as $c_{p/q} = \frac{e^{2\pi ip/q}}{2} - \frac{e^{4\pi ip/q}}{4}$ [2.5a].

To find the equation of the period 2 bulb, we look for a fixed point of the second iterate: $f^{(2)}(z) = (z^2 + c)^2 + c = z$. Solving for c we have: $c^2 + c(2z^2 + 1) + (z^4 - z) = 0,$

$$\text{or } c = \frac{-(2z^2+1) \pm \sqrt{(2z^2+1)^2 - 4(z^4 - z)}}{2} = \frac{-(2z^2+1) \pm 2z + 1}{2} = z - z^2,\ -(z^2 + z + 1)$$

The first solution is the period 1 cardioid since $z^2 + c = z$ . The second solution gives $z^2 + c = -z - 1, \text{ or } z^2 + z = -1 - c$.

$$e^{i\theta} = f^{(2)}{}'(z) = 4z^3 + 4cz = 4z(z^2 + c) = -4z(z+1) = -4(z^2 + z) = -4(-1 - c),\ c = -1 + \frac{e^{i\theta}}{4} \quad [2.6]$$

A circle of radius ¼ centered at -1 as per fig 3.

However to get the full picture, we need to figure how to turn a deeply enigmatic topological criterion into a computable algorithm, and here is where the heart of fractal complexity really hit the fan.

If we consider $f(z) = z^2 = \left(r(\cos\theta + i\sin\theta)\right)^2 = \left(re^{i\theta}\right)^2 = r^2e^{2i\theta}$ [2.7], we find that numbers outside the unit circle get larger with the square of the radius (modulus) and tend to $\infty$, while those inside tend to 0.

The points on the unit circle are trapped at modulus 1 and become the Julia set, forming a repelling crest between the two basins of the attractors 0 and $\infty$. Since the angle (argument) of each point is doubled under [2.7], on the unit circle we have $g(\theta) = 2\theta$ [2.8], and after $n$ steps $g^{(n)}(\theta) = 2^n\theta$.

This process is chaotic, satisfying three chaotic properties [2.9]:
(1) *Sensitive dependence:* Since angle is repeatedly doubling, the process has the butterfly effect – there exist points arbitrarily close which get mapped globally apart after a finite number of steps through.
(2) *Topological transitivity:* Any small open region (angular interval) is eventually expanded over the whole circle overlapping every other small open region so it has topological mixing.
(3) *Dense periodicities:* The dynamics is permeated with (repelling) periodic points as close as we like to any other point. Solving $g^{(n)}(\theta) = \theta$ [2.10], we get $2^n\theta = \theta + 2k\pi$, or $\theta = \frac{2k\pi}{2^n - 1}$, $k = 1, \mathsf{K}, 2^n - 1$ [2.11], i.e. $2^n - 1$ evenly spaced points of period n, which are all repelling, since $g'(\theta) = 2 > 1$.

These are the three axioms of chaos demonstrated.

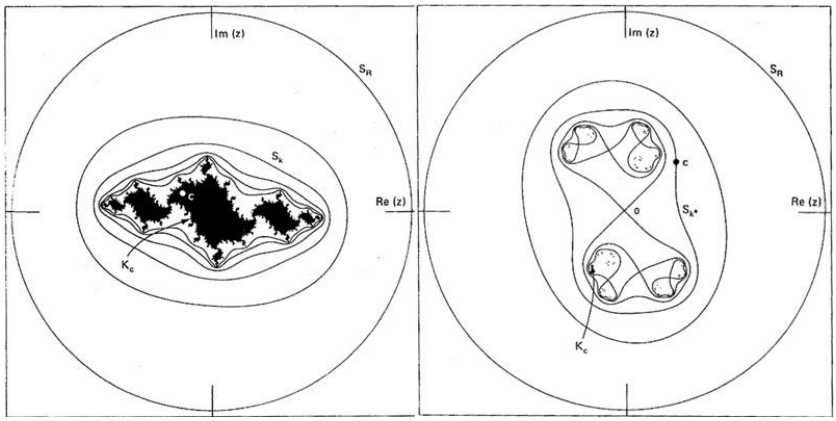

Fig 4: Inverse images of a large circle in (a) the connected and (b) disconnected cases (Peitgen et. al. 1988).

Now let's go back to $f(z) = z^2 + c$ and look at the function on a very large circle, as in fig 4. Here $z^2$ is much larger than $c$, so it's essentially mapping a circle to an even larger circle. The point at infinity is a super-attracting fixed point and the Julia set is the boundary of its basin of attraction. Now take successive inverse images of this circle. By continuity, these must be continuous closed curves and they have to come to one of 3 cases: (i) a single topological circle (simple closed curve) with two points rotating around it as the two solutions of $z_n = \pm\sqrt{z_{n+1} - c}$ [2.12] as c varies on the original circle, or (ii) two separate circles each with one solution or (iii) a transitional case of a figure 8 (or figure $\infty$!). We can't have any other cases like two circles overlapping at 2 points because this would cause a repeated root at each crossing and hence 4 roots when we only have a degree 2 quadratic with 2 roots, whose repeated root, from [2.12], is 0.

If the inverse images are all topological circles, then the filled in Julia set $K_c$ must be connected, as in fig 4(a), as the circles and their inverse images form an effective conformal mapping of the plane minus a disc onto the plane minus the filled in Julia set. On the other hand, if we do have a first figure 8, we have a repeated root i.e. $z = \pm\sqrt{0} = 0$, and $f(z) = f(0) = c$ [2.13], so $c$ is on the last circle whose inverse image (a figure 8) is connected and $c$'s inverse image is 0 on the figure 8, as shown in fig 4(b). In the connected case we never reach $c$, so it is inside the filled in Julia set and thus 0 must stay confined inside when iterated. By contrast, in the disconnected case, 0 will iterate to $\infty$ and eventually escape any fixed large circle. Notice that $z = 0$ is the critical point of $f(z) = z^2 + c$, as $f'(z) = 2z = 0 \Leftrightarrow z = 0$ [2.14].

The critical point is the acid test because it is the last point to escape iterations, since the function is stationary there.

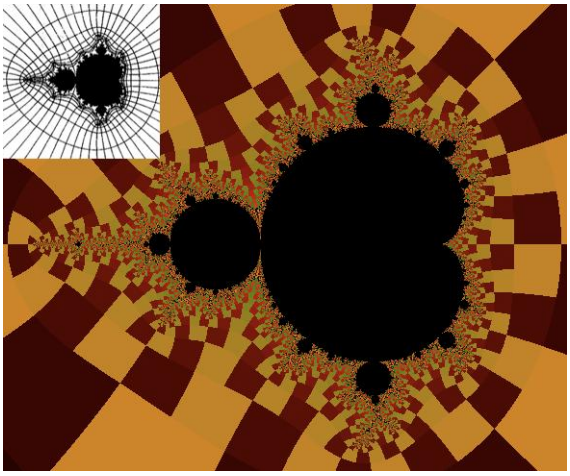

Fig 5: (Inset) The Mandelbrot set can be proved connected by extending the mapping beyond c to the entire complement of M, resulting in a conformal mapping between the complement of M and the complement of a disc, corresponding to radii and angles of the standard potential function around the unit disc. This is illustrated by using a binary decomposition in which the level sets are chequerboarded by whether the escaping n-th iterate is in the upper or lower half plane - i.e. has poisitive or negative imaginary part.

The quadratic Mandelbrot set can also be shown to be a connected set by extending the above conformal mapping arguments for Julia sets in the region outside $c$ to a conformal mapping over all regions where $c$ is outside M, as shown in fig 5.

We now have a computable method for finding the Mandelbrot set of any one-parameter quadratic family: Iterate $z_{n+1} = f_c(z_n),\ z_0 : f'(z_0) = 0$ [2.15], for each point $c$ in the complex plane. If it remains inside a given large circle after a fixed number of iterations, colour the point black, otherwise colour it with the number $n$ of steps to escape. This is the level set method. It leaves the Mandelbrot set black with its complement a coloured topographical dynamic landscape – hence the 'dark heart'. It is also used to picture the exterior of a Julia set $J_c$ by starting from each point $z_0$ in the plane for fixed $c$. We will use this method to investigate the properties of Julia sets and the Mandelbrot set of a variety of functions. One can also, with some greater difficulty, attempt to shade the interior basins of the Mandelbrot and Julia sets, by counting how many steps the iteration takes to get within a small neighbourhood of any attracting periodic points, as illustrated in the Julia sets of fig 1 and the Mandelbrot set of fig 3. However this fails if the Julia sets contain neutral points.

One can also colour the complement of Julia and Mandelbrot sets with a continuous potential, by comparing the potential of the $n$-th iterate $z_n$ escaping a large circle with the standard 2D logarithmic potential $p = \log(r)$ [2.16], using the function

$$Pot_c = \frac{\log|z_n|}{2^n} \quad [2.17]$$

We can also picture the rays corresponding to external angles, $k/2^n$, measured in fractions of a revolution, of the dynamic rays of potential function by colouring $c$ black or white, according to whether the escaping $z_n = f_c^{(n)}(0)$ lands in the upper or lower half plane, called a binary decomposition. The $2^n$ factor comes from the repeated angle doubling of $z^2$ which is dominant on large circles. The method turns fig 5 into a checkerboard pattern highlighting segments of both rays and level curves.

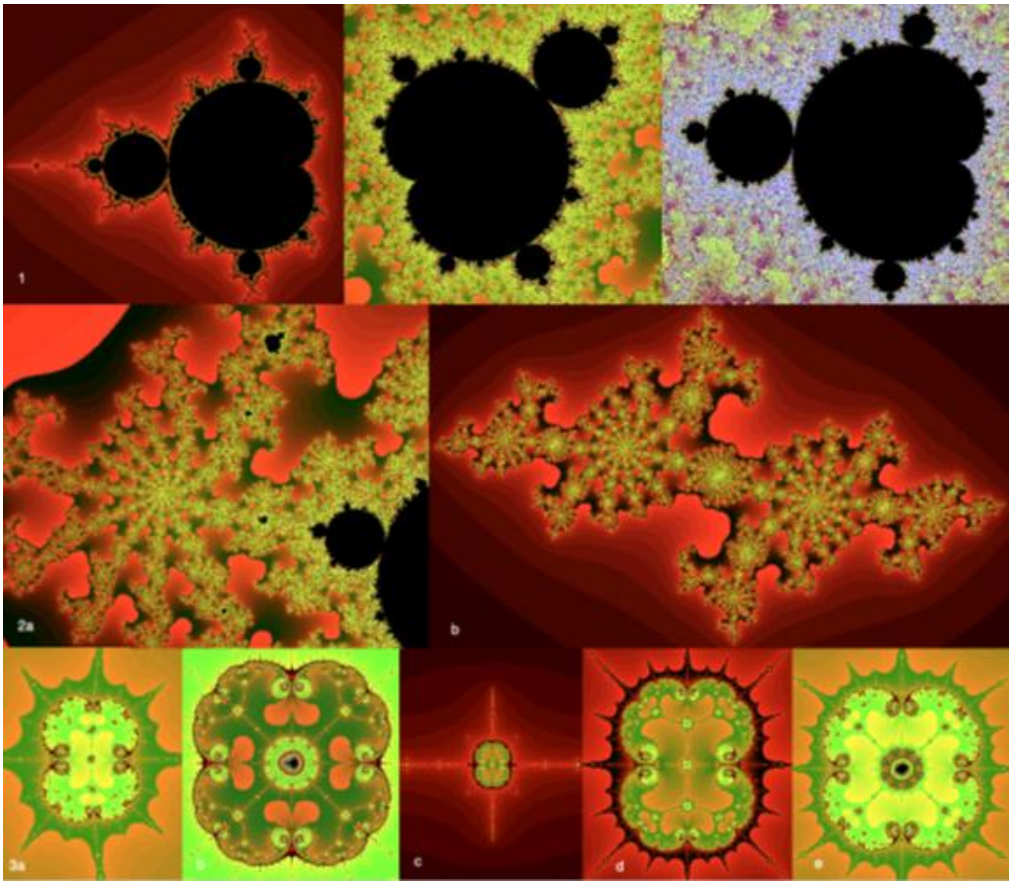

Fig 6: (1) Parts more complex than the whole – the fractal black hearts, connected to the main body by dendrites, get warm and fuzzy on blowup, since the dendrites become locally space-filling as the Farey denominators tend to infinity. On descending fractal scales the Mandelbrot set boundary fills 2-D space and thus has fractal dimension 2. (2) Locally varying complexity. The Mandelbrot dynamics in each locality (a) captures the dynamics of each corresponding Julia set (b). (3) Embedded Julia set (a) in the intermittency crisis region of the main period 3 island on the period 2 dendrite with (b) central small island. (c) Corresponding Julia set with fractal embedded homologs (d) each with a period 1 Julia set in their core (e) corresponding to the period 1 region of the small Mandelbrot island (b).

As an atlas of all the varied complex dynamics in the entire family, the Mandelbrot set is sometimes regarded as the most complicated mathematical object in existence. The local dynamics at any point $c$ on the Mandelbrot atlas closely represent those of the corresponding Julia set $J_c$ (Tan ), as shown in fig 6. Although it was only proven in 1991 (Shishikura), the Mandelbrot set boundary has fractal dimension 2, the same as the plane it sits in, essentially because the number of dendrites grows to $\infty$, in such a way that the boundary locally forms a space-filling tree, because the Farey denominators (see next section) of the dendritic islands increase without bound, as we descend down fractal scales (fig 6). It is not known whether this results in a boundary of non-zero area.

A convenient way of completing the complex plane so that the iterations are consistent with a single point at infinity is to close it off into a sphere, called the Riemann sphere, with the single point at infinity at the north pole, the unit circle as the equator, and the origin at the south pole, mapping all points in the plane by stereographic projection from the north pole. This way the point at infinity can be treated like any other point.

If we now turn back to the equation we started with – the logistic iteration $f(z) = cz(1-z)$ [2.18] – although the global form of its Mandelbrot set is apparently different, both the period multiplying bulbs and

the dendritic islands, and the local dynamics and forms of the Julia sets are all homologous with those of the standard function $f(z) = z^2 + c$.

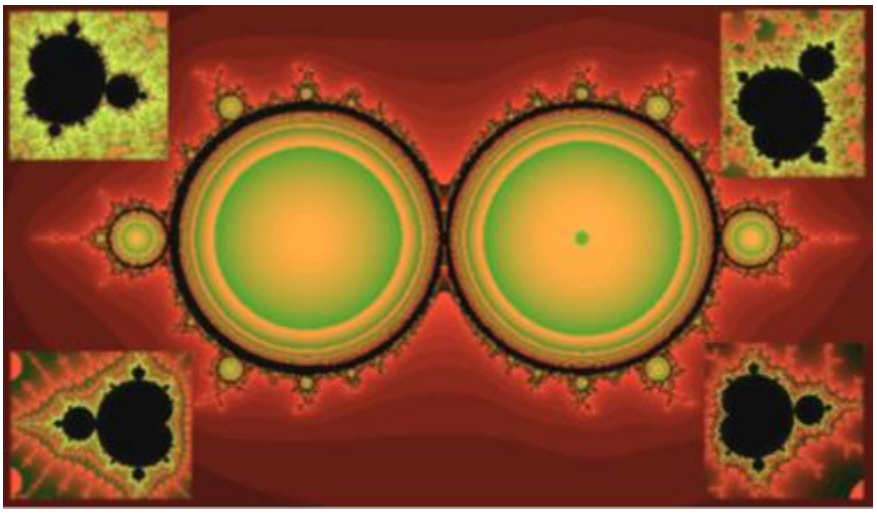

Fig 7: Although the parameter plane of $f(z) = cz(1-z)$ consists of two circles forming a pair of the quadratic period doubling bulbs on the standard Mandelbrot set, its dendritic islands have the same cardioid as $f(z) = z^2 + c$. The inside of the set is shaded by approach to its internal periodic attractors.

To generate an image of the parameter plane we replace the origin with the correct critical point. Solving $f(z) = z,\ f'(z) = e^{i\theta}$ for $c$ in terms of $\theta$ gives:

$$f(z) = cz - cz^2 = z,\ z\big((c-1) - cz\big) = 0, f'(z) = c - 2cz = e^{i\theta}$$
$$z = 0,\ c = e^{i\theta};\ z = (c-1)/c,\ -c + 2 = e^{i\theta},\ c = 2 - e^{i\theta} \qquad [2.19]$$

This gives two solutions representing the left and right unit circles in fig 7 centered on 0 and 2, respecting the essential symmetry in the function between $z$ and $1 - z$, while the roots are 0 and 1 and the critical point is 1/2. Each of these two major regions of the parameter plane is of course a perfect copy of each of the bulbs on the periphery of all versions of the black heart. We can derive the circular equation 2.6 for the period 2 bulb of $f(z) = z^2 + c$ (see appendix 1), however, the higher periodicity bulbs, despite being obvious circles, have intractable solutions, because quadratic period $n$ corresponds to solving a polynomial of degree $2^n$, which is impossible classically for degree greater than 4. Effectively the parametrization has created a bilinear map, giving a pair of degree 1 circular 'hearts', which only show their true quadratic nature on fractalization, but give us a quick window into the equations for the circular bulbs.

Intriguingly, the equation [2.5] connecting the unit circle to the cardioid, is also expressed between the parameters of $f(z) = z^2 + c$ and $f(z) = rz(1-z)$ in the form $c = \frac{r}{2} - \frac{r^2}{4}$ [2.20], precisely conjugating the sequence of their bifurcations on the real axis. For example first period doubling 3 maps to -3/4 and the tip of the main dendrite maps 4 to -2.

### 3. The Dark Heart's Magic Numerology

In fig 8 are shown three classical routes from order to chaos. The first – period multiplying – a generalization of period doubling, requires an infinite sequence of bifurcations, arriving in limit at a strange attractor (Schröder) and chaos. The strange attractor for the real mapping of fig 1 is shown as

$r^{\infty}$ and the corresponding Julia set above has a central black area highlighting this strange attractor, contrasting with the generally 'repulsive' nature of the Julia set under the forward mapping. By contrast with the real number period doubling route, a journey to the dendrites of the dark heart can involve any sequence of periodicities determined by which bulb is entered. This complicates the expression of Sarkovskii's theorem, which also doesn't actually describe the full order of the periodicities, as we shall see shortly. As we move along any dendrite of any compound period, we will go through a transition similar to the real transition after $r^{\infty}$ in fig 1. The dendrites have the base $n$ periodicity of the local process, but as we move out along them, they are fractally permeated by a tree of dendritic Mandelbrot islands with varying fundamental periods, each of which is capable of generating new components of any periodicity on its bulbs.

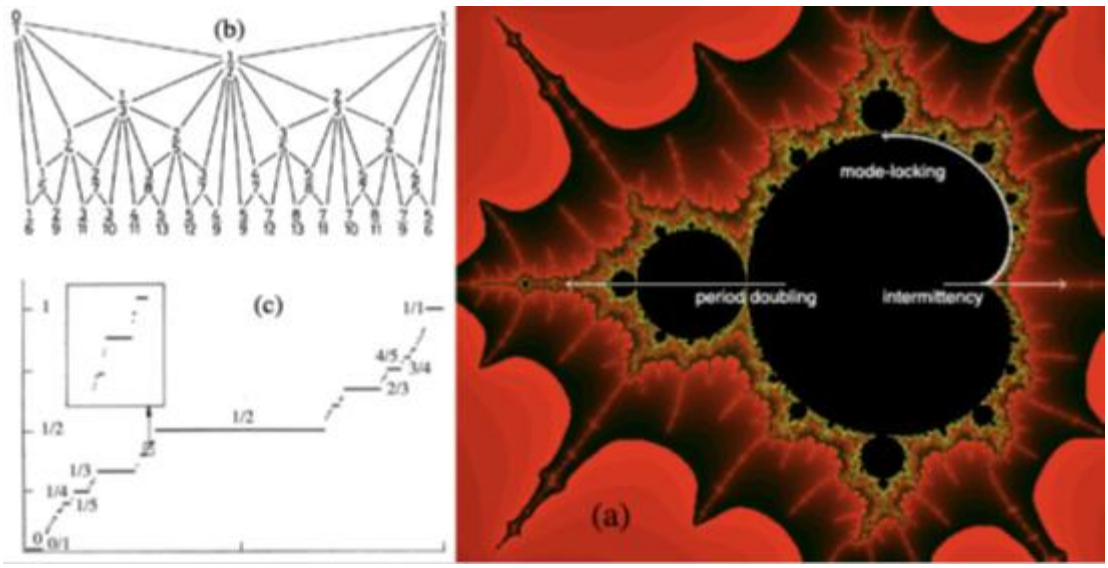


Fig 8: (a) The three routes to chaos illustrated on the real axis period 3 dendritic island of the black heart of the level set method, (b) the Farey tree of winding numbers and dendrites of the bulbs, (c) the Devils' staircase of mode-locking.

The second – intermittency crisis – illustrated in fig 2, involves switching between periodicity and chaos in a single bifurcation, as shown in fig 1 at 3.8282 just to the left of period 3 because part of the graph of $G^{(3)}(x)$ crossing $y = x$ has become tangent and then separated allowing intermittent slippage of the period 3 into chaos. The same transition is responsible for the exploding transcendental Julia sets we will look at later.

All dendritic processes on the Mandelbrot set go through repeated fractal transitions through black hearts, firstly following reverse intermittency-crisis, and then period-multiplying, as we move out along the fractal dendrites. All parts of the complex structures in the dendrites consist of fractal branching arcs of the periodicity of the bulb from which they protrude, interconnected by black hearts, where the periodicity on the dendrite undergoes further multiplication. In the related Julia set, the black hearts are replaced by structures of the periodicity, or transition dynamic, corresponding to the Julia set, also possessing the basic $180^{o}$ rotational symmetry of quadratic Julia sets.

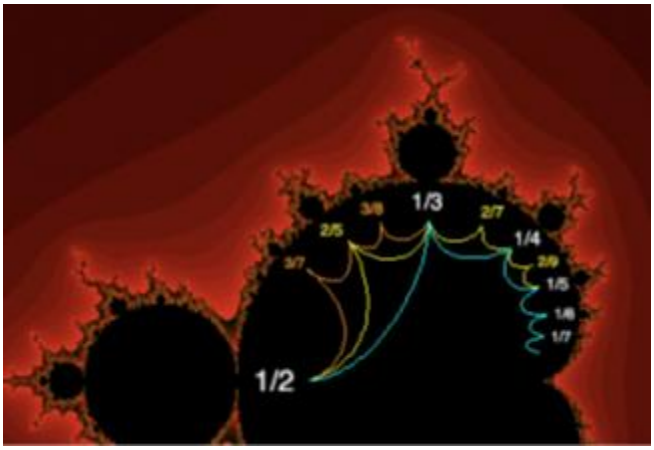


Fig 9: Mode-locking bulbs follow an decreasing sequence of fractional rotations by 1/$n$, with all the remaining rational fractions generated in between as mediants.

In the third process – mode-locking – any irrational local dynamic close enough to a rational fractional rotation undergoing dynamical feedback becomes locked to the periodicity of that rotation, forming a series of intervals of mode-locked states, with only a residual set of points in between retaining their unperturbed irrational motion. These mode locked intervals form a continuous fractal ascending (monotone increasing) function, constant on intervals surrounding rationals, called the Devil's staircase as in fig 8(c). Mode-locking is manifest in many processes where periodicities interact, including the non-mode-locked orbits (to Jupiter) of the remaining asteroids, because the mode-locked ones were thrown into chaotic orbits and collided with planets, the ordered mode-locking of the Moon's day to the month and Mercury's day to 2/3 of its year.

As shown in figs 3, 9 the bulbs on the Mandelbrot set follow the fractions on the Farey tree in fig 8(b), adding fractions as mediants $\frac{p}{q}+\frac{r}{s}=\frac{p+r}{q+s}$ [3.1], as can be seen by counting the number of their dendrites, which also corresponds to the periodicity of the attractor corresponding to the main bulb. Mediants correctly order the fractional rotations between 0 and 1 into an ascending sequence providing a way of finding the fraction with smallest denominator between any two other fractions. A way of seeing why this is so is provided by using a discrete process to represent the periodicities or fractional rotations. For example if we have 2/3 =110 and combine it with 1/2=10 by interleaving, we get 11010, or 3/5.

Numbers like the Golden Mean $\gamma=\frac{-1\pm\sqrt{5}}{2}=0.618,-1.618$ [3.2], which by virtue of its defining relation $\frac{1}{\gamma}=1+\gamma$ [3.3], is the limit of the ratios of successive Fibonacci numbers 1, 1, 2, 3, 5, 8, 13, 21 … for which $F_{n+1}=F_n+F_{n-1},\ F_0=F_1=1$ [3.4] are non-mode-locked. The Farey tree leads to Golden Mean numbers, if we alternate left and right as we go down, following a series of Fibonacci fractions. Numbers $g$, such as these, avoid becoming mode-locked because their distance from any fraction of a given denominator $q$ exceeds a certain bound: $\left|g-\frac{p}{q}\right|>\frac{\varepsilon}{q^2},\ \ \varepsilon:\ \frac{1}{\sqrt{5}}$ [3.5].

The golden numbers can most easily be described in terms of continued fractions, which, when truncated represent the closest approximation by rationals: $n=a_0+\cfrac{1}{a_1+\cfrac{1}{a_2+\cfrac{1}{\mathsf{L}}}}=[a_0,a_1,a_2,\mathsf{K}\,]$ [3.6].

Golden numbers end in a series of 1's thus having slower convergence to fractions of a given denominator than any other numbers. The Golden Mean itself is $[1,1,1,\mathrm{K}]$ [3.7]. More generally, the Farey Tree has straightforward natural rules of parental and descendent inheritance, using continued fractions and any fraction or quadratic rational has a repeating continued fraction (Schröder).

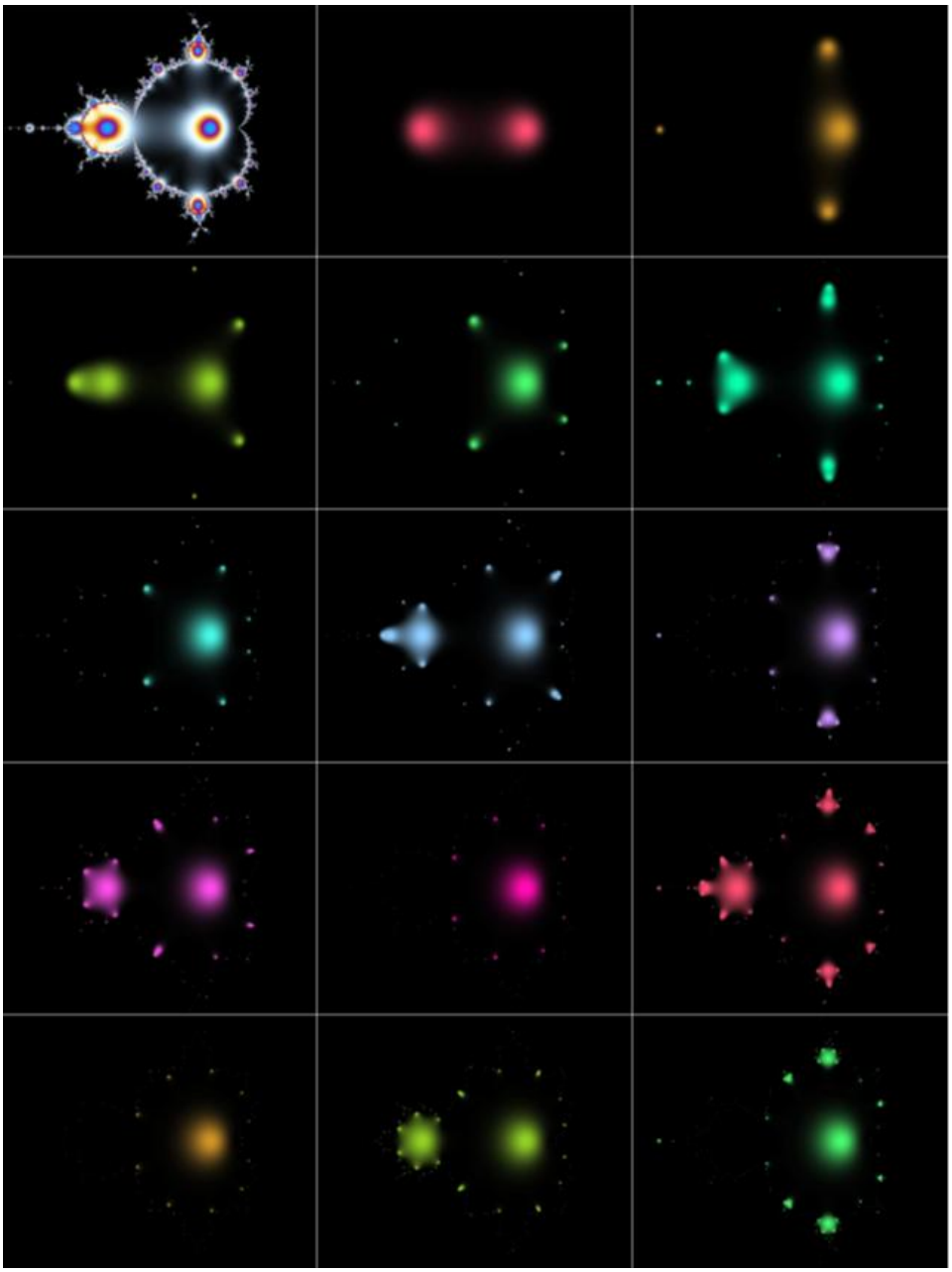

Fig 9b: Locations of the periodic bulbs and Mandelbrot dendritic islands for periods $n$=1-15, located by Gaussian wave function method. Images of non-prime $n$ include all factor periods. Top-left image is a superposition of periods 1-101.

All the Julia sets on the cardioid boundary are caught on bifurcation out of period 1 and fall into rational and irrational types. The rationally indifferent or mode-locked Julia sets such as 2 and 8 in fig 3 (called parabolic) have neutral points which are in the Julia set (compare the attracting fixed point in 1), because they have $n$ repelling branches, as well as $n$ attracting petals, forming an $n$-branched saddle point. After

bifurcation the $n$ petals form the components of a period $n$ basin, corresponding to the periodicity of the adjacent bulb, as in 4. By contrast the irrationally indifferent Julia sets have a neutral point in their internal basin, around which all the points in the basin are irrationally rotating.

One of the most challenging features of the Mandelbrot set is the bewildering arrangement of the dendritic Mandelbrot 'islands' which are strung like Indra's beads along the dendrites, playing a key role in introducing higher periodicities and causing the fractal dimension of the boundary to be space-filling in the plane.

One way of visualizing the precise locations of all the $2^n$ periodic bulbs and dendritic islands of a given period $n$ is to use the wave function method described in appendix 1 with a radial function coloured by sines and cosines of a Gaussian distribution, viz

$$ColorM(y,x,i) = \left|\cos\left(\frac{2\pi n}{k_1} + \frac{\pi i}{4}\right)\right| * \mathrm{e}^{-k_2|z_n|^2},\ i = r,\ g,\ b\ .$$

Douady and Hubbard discovered a number of intriguing relationships depending on the critical point that index the features of the bulbs and their dendrites in terms of the critical points. These depend on the external angles, the angle of the ray from the unit disc that corresponds to each ray in figs 5,10. There are intriguing ways to calculate these angles both for the bulb cusps and key points on the dendrites.

Inside each period-$n$ bulb is a central super-attracting point, where $f_c^{(n)}{}'(z_i) = f_c'(z_1)\,o\,\ldots\,o\,f_c'(z_n) = 0$ [3.7] for any point on the period-$n$ cycle. But this means that one of the derivatives $f_c'(z_i)$ has to be zero, so $z_i = 0$ the critical point. Hence the critical point is periodic with period $n$ at this $c$ value. Hence there is a point $c$ in each bulb where $f_c^{(n)}(0) = 0$, resulting in an equation of degree $2^{n-1}$. For example for period 3, we get $(c^2+c)^2 + c = c(c^3 + 2c^2 + c + 1) = 0$ [3.8] , giving the period 1 heart and the three locations of the small period 3 dendritic Mandelbrot island on the main dendrite and the two period 3 bulbs above and below the main heart.

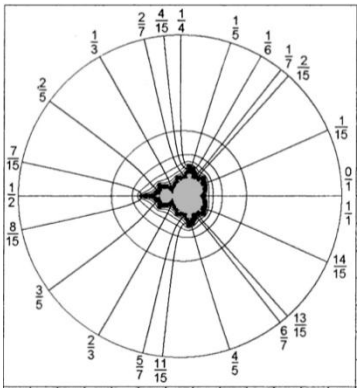


Once we exit the bulbs and enter the dendrites, the fundamental periods become repelling and the critical point becomes eventually periodic to a repelling periodic orbit of period $k$ after $n$ steps, at Misiurewicz points $M_{n,k}$, the tips and branching points of all dendrites. For example for $M_{2,1}$ we have $(c^2+c)^2 + c = c^2 + c$ [3.9], giving $c$=0 (where the critical point is fixed) and $c$=-2 the tip of the main dendrite.

Fig 10: A collection of dynamic rays with their external angles (Pastor et. al. Romera et. al.)).

It is possible to calculate the external angles of a variety of key points on the boundary of the Mandelbrot set by an ingenious method which depends on the squaring nature of the quadratic to form exterior angles over powers of 2 using the upper and lower half plane as a discriminating target as noted in the binary decomposition.

If we consider a critical point in either a periodic orbit or an eventually periodic orbit, we can encode the dynamics as a binary 'decimal' setting a 0 for each iterate in the upper half of the local traverse of the 0/1 and 1/2 rays, which are asymptotic to the positive and negative real axis. When we expand this decimal as a power series it gives the external angles of the cusps of the bulbs and dendritic Mandelbrot islands and the Misiurewicz dendrite tips and branching points.

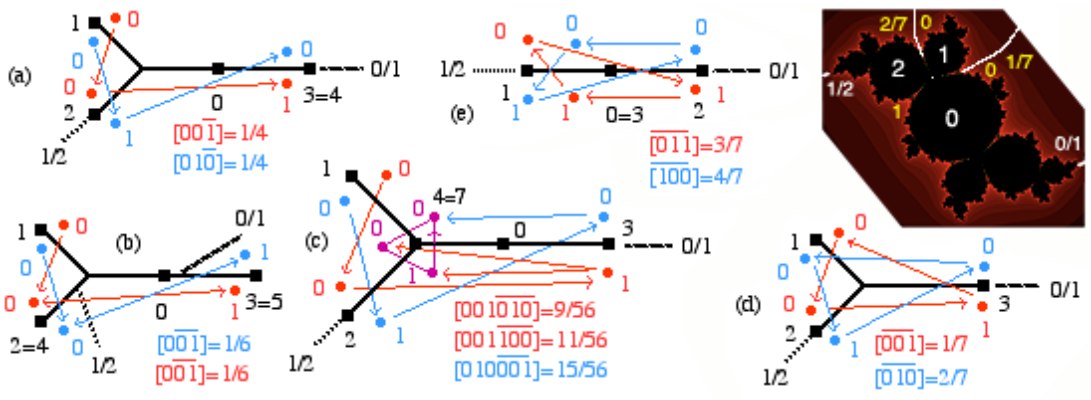


Fig 11: Calculation of the external angles of several key period-3 points. We start with the first iterate (1) and assign 0 or 1 if a given iterate is above or below the traversal between the connections between the 0/1 ray and the 1/2 ray: (a) The $M_{3,1}$ at the tip of the largest period 3 dendrite. (b) The $M_{3,2}$ at the tip of the second period 3 dendrite. (c) $M_{3,3}$ the main branching point of the period 3 dendrite. (d) The super-attracting period of the period 3 bulb gives the exterior angles of the two cusps, confirmed by cusp Julia set rays above. (e) The exterior angles of the cardioid main cusp on the period 3 Mandelbrot island on the period 2 dendrite. The ray 0/1 is the preimage of edge 01. Ray 1/2 is the preimage of 0/1. In (b) 03 is the preimage of 14 so the preimage of 01 must extend from 03 at an angle. In (c) the ambiguity in the orbit [001***] provides the third exterior angle.

Rays emerging from cusps and dendritic islands all have external angles fractions of the form $\frac{k}{2^n-1}$ [3.10] because of the repeated binary decimal associated with their periodicity. E.g. $\overline{00\text{L}\ 01} = \sum_{i=1}^{\infty} 2^{-in} = \frac{2^{-n}}{1-2^{-n}} = \frac{1}{2^n-1}$ [3.11]. Furthermore these lead to every odd denominator fraction as a result of Euler's generalization of Fermat's little theorem $a^{\varphi(n)} \equiv 1 \bmod n$ where $a$, $n$ are coprime and $\varphi(n)$ is the number of integers less than $n$ coprime to $n$. For example for 9 we have 1, 2, 4, 5, 7, 8 give $\varphi(9) = 6$, so $\frac{1}{9} = \frac{7}{63} = \frac{7}{2^6-1}$ and $\frac{1}{9}$ is actually an external angle of the period 6 bulb.

By contrast, those from Misiurewicz points have even denominators because the non-periodic initial iterations cause an irreducible power of 2 in the denominator.

There are also some intriguing irrational angles. The sequence of period doubling points have sequences $[\overline{01}] = 1/3, [\overline{0110}] = 2/5, [\overline{01101001}] = 7/17$ [3.12], tending to the Morse-Thule fractal sequence in, which we invert each binary decimal and append it to the right. There are a corresponding sequence of rays emerging from the Misiurewicz points $M_{2^n,2^{n-1}}$, $[01\overline{10}] = 5/12, [0110\overline{1001}] = 33/80, \text{L}$ [3.13] also tending to the same limit equivalent to $r^{\infty}$ in fig 1. Further codings can be found in Pastor (2002).

From Sarkovskii's theorem, we gained an idea of the way the periodic windows form odd and period-doubling series, which from fig 1 correspond to dendritic Mandelbrot islands in the complex case. However Sarkovskii's theorem doesn't actually tell us which period windows occur and in which order and there are clearly more than the sequence indicates, for example a further period 5 window to the right of 3. In fact the distribution of these is encoded in the eventual (*k*,*n*)-periodicities of the Misiurewicz points, in turn encoded by rational external angles. However we need to have a more direct idea of where these periodicities occur.

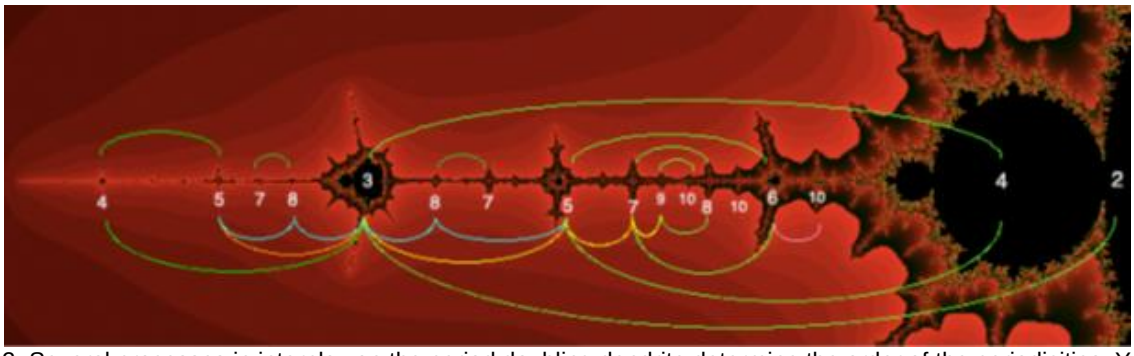


Fig 12: Several processes in interplay on the period doubling dendrite determine the order of the periodicities. Yellow links show the first members of the odd Sarkovskii series 3, 5, 7, 9 and in mauve the first two of the period doubled odds 6, 10. Green, linked by increasing steps of 1 from 2 to 10 is the main period winding sequence. In orange is a mirror odd sequence 3, 5 leading to a further fractal winding sequence. Blue links are mediant-generated periodicities as in mode-locking. The winding sequences are generated through period 2 dividing the periods into even (0 mod 2) and odd (1 mod 2) creating two ascending series of Mandelbrot dendritic islands with base periodicities covering all the natural numbers above 2 and their fractally entwined recursions repeating the sequence from higher levels.

To make some sense of this while writing the paper, I investigated the base periods of the collection of dendritic Mandelbrot islands illustrated in figs 12 and 13. The sequence of periodicities in fig 12 standing alone are enigmatic and appear both random and repetitious, however once we elucidate the patterns in periods 3 and 5, we can begin to see both a generalization and several interpenetrating processes determining the overall structure.

Firstly, instead of period 2's odd series and even doublings, we have $n$ classes corresponding to the residues mod $n$, corresponding to the $n$ fractal dendrites, each of which has an ascending sequence in steps of $n$ with the $k$-th residue remaining constant on a given arm, forming $pn+k,\ k=0,\mathrm{K}\ ,\ n-1$ [3.8]. The base arm consists of the multiples of the base periodicity. This means that an island exists with every base period above the base bulb's periodicity, winding in to the hub of the main set of $n$ spokes. A second reflected series occurs running out along each dendrite from the dominant island. In addition mediant periodicity addition occurs, resulting in fractal extension of the process, as illustrated in fig 13.

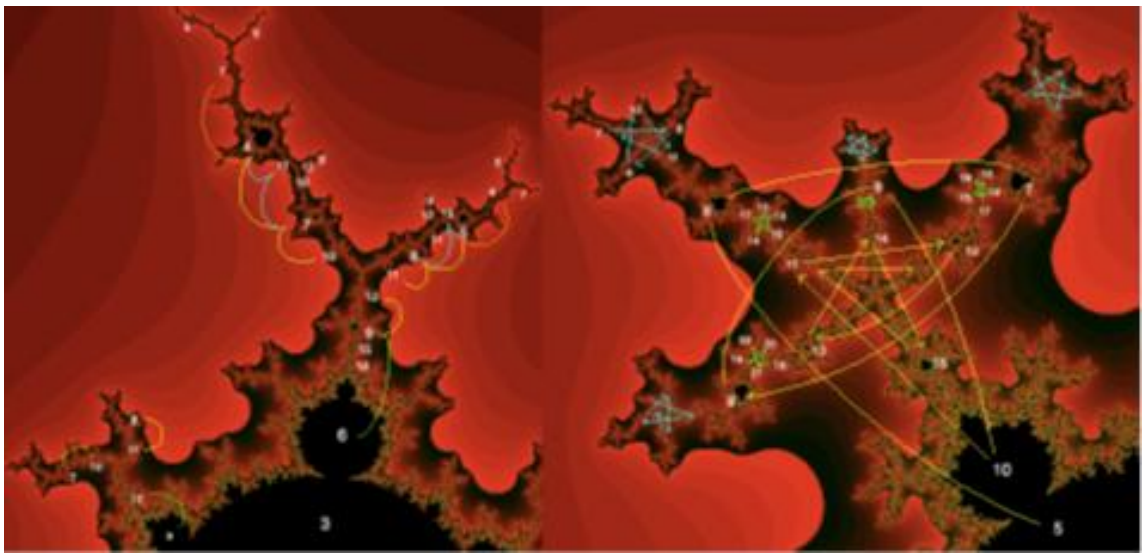

Fig 13: Period 3 and 5 dendrites (1/3 and 2/5 a revolution) show the fractal effects of mediant formation and period winding with periods of all orders, strung in ascending series following the base period $n$ of the bulb, in such a manner that the $k$-th of the $n$ arms are composed of periodicities $pn+k,\ k=0,\mathrm{K}\ ,n-1$, with the base periodicity and first period doubling bulb forming members of the sequence. (Left) Period 3 showing in yellow mod(3,1) and mod(3,2) branches 4, 7, 10 and 5, 8, 11 and the periods 6, 9, and 12 on the main dendrite forming a period doubled set. In orange a reflected $n$ step series running outward. In cyan, additive period mediants, 11 of 4 and 7 and 13 of 5 and 8, are located between the associated triple branching and the next Mandelbrot dendritic island, with the $n$-1 other associated periods forming a fractal version of the main winding sequence. Far left the corresponding sequences of the period 9 sub-bulb follow the same pattern. (Right) Fractal winding sequences on period 5 dendrite, with 2/5 of a revolution, each rotate by two vertices, forming a pentagram spiral, with fractal recursions on each branch (cyan and green).

Given the ray angles forming a continuous circle, there are clearly points on the Mandelbrot set corresponding to every possible binary 'decimal' angle. So we can characterize all points on the boundary in terms of their sequences, periodic, eventually periodic or irrational. Clearly although the rational numbers are dense the irrational numbers constitute real rather than countable cardinality and thus the countable collections of bulbs, islands, and M-points we are examining only form the occasional stars in a mysterious irrational sky of boundary points, with a few additional irrational limit points thrown in.

If we use the binary sequence corresponding to a given ray, we can immediately see sequences which correspond to Mandelbrot islands, decoding their ordering and periodicity.

For example beginning with the period 2 bulb and its dendrite, we have the sequence of periods 2, 3, 4,…, $n$, stepping from the period 2 bulb to the main period 3 island and then out, converging to the eventually periodic tip point $M_{2,1}$: $[\overline{01}],\ [\overline{011}],\ [\overline{0111}],\mathrm{K}\ ,[0\overline{1}]$. Each of these is a period $n$ island because it is periodic and its external angle places it on the period 2 dendrite.

There are then period doubling versions of this sequence of periods 4, 6, 10, … , 2$n$ converging to the $M_{3,1}$ point: $[\overline{0110}],\ [\overline{011010}],\ [\overline{01101010}],\mathrm{K}\ ,[01\overline{10}]$. Although this point has eventual periodicity 1, the map is flipping half-planes here, so it is the period 2 'band merging' point with sequence $[01\overline{10}]$ corresponding to the main M-point junction of $n$ dendrites of a period $n$ bulb. This period doubling sequence of sequences continues, in steps of $2^n$, with M-point limits converging to the Morse-Thule sequence of the period doubling $r^\infty$ point, as noted above.

We can also see periodicities 3, 5, 7, … , 2$n$+1 forming a sequence of islands to the right of the period 3 island converging to the same 'band merging' point: $[\overline{011}],\ [\overline{01101}],\ [\overline{0110101}],\mathrm{K}\ ,[01\overline{10}]$, and again period doubled versions of these, consistent with the bifurcation diagram of fig 1.

If we put this together with the even sequence $[\overline{01}],\ [\overline{0110}],\ [\overline{011010}],\ [\overline{01101010}],\mathrm{K}\ ,[01\overline{10}]$, which also converges to the same 'band merging' point, we get the main winding sequence of periods 1, 2, 3, 4, …, $n$ of fig 12: $[\overline{01}],\ [\overline{011}],\ [\overline{0110}],\ [\overline{01101}],\ [\overline{011010}],\mathrm{K}\ ,[01\overline{10}]$.

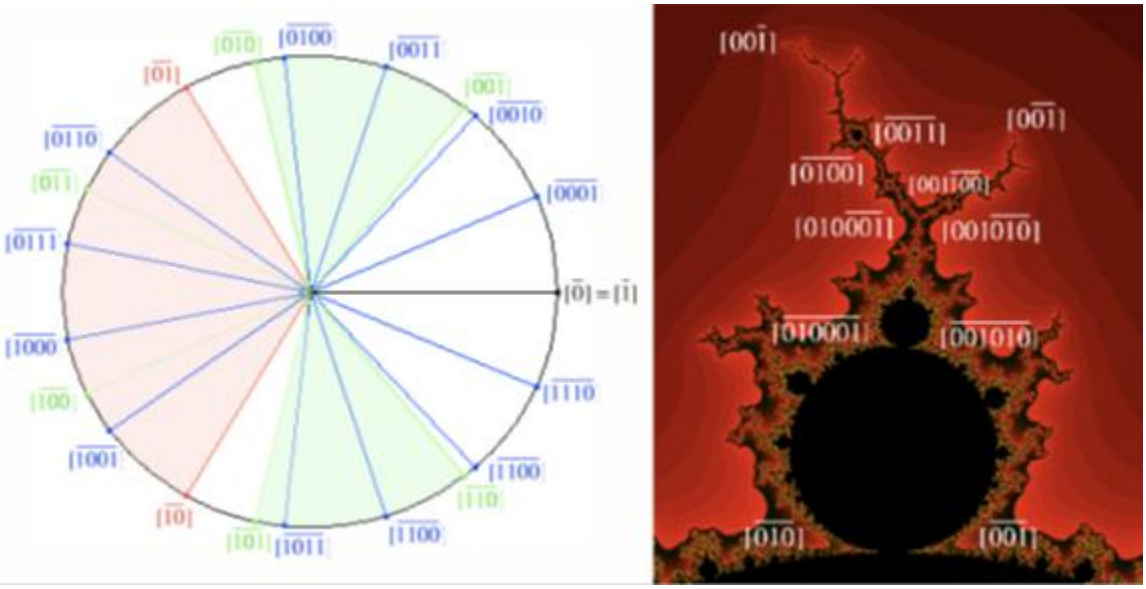


Fig 13a: Left Periods 1, 2, 3, 4 (black, red, green and blue rays) on the circle map diagram, with the sectors clamed by periods 2 and 3 bulbs shaded. Looking at period 4 clockwise from 0, the first two rays form the cusps of the main period 4 bulb, the next 2 from the period 4 island on the main period 3 dendrite, the next is period 2, leaving two ray pairs in the period 2 sector, the period 4 period doubling rays and the rays from the one period 4 island at the tip of the dendrite.

We can now begin to think about finding the position of a given ray sequence on the boundary of the Mandelbrot set. Now to see where these actually might be we need to consider the way the sequence of lower periodicity bulbs and islands carve out ray parameter space in a manner similar to the devil's staircase. The easiest way to see this is to look at the disc from which the rays emerge and to consider the periodicities in terms of the angle doubling circle map corresponding to $z^2$. Recall from [2.11] that this has a dense set of $2^n-1$ periodic points of period n, with angles $k/(2^n-1),\ k=1,\mathsf{K},2^n-1$ coinciding with our external angles. For example for n=2 there are two period 2 points $2\pi/3$ and $4\pi/3$, mapping to one another, and 1 which is period 1, together forming an equilateral triangle about the origin. Moreover the eventually periodic points to any period are also dense. For example there are $2^n$ points eventually fixed to 1, since $g^{(n)}(\theta)=2^n\theta=0+2k\pi,\ \theta=\dfrac{2k\pi}{2^n}$.

In fig 13a, period 1 is in black, period 2 in red, 3 in green and 4 in blue. We can now analyse the positions of all the period 4 bulbs and islands. Counting round clockwise from 0 as in fig 13a, we find firstly the arcs from the main cardoid period 4 bulb (the only one on the cardioid of this period), next because the two arcs ar in the period 3 sector this must be the period 4 island on the main dendrite, next is a period 2 ray, followed by two ray pairs centered on ½, forming firstly the arcs above and below the first period doubling period 4 bulb and second those emerging above and below the main cusp of the one period 4 island on the period 2 dendrite.

More generally, we can decode any period-$n$ sequence by examining whether the ray (or ray pair) falls within any of the sectors of the main bulbs of periods 1, 2, …, $n$-1. If not it is a main bulb. If it does fall in a lower period sector, we can analyse it's address further, using key landmarks on the bulb concerned. For example, we know the period 4 island is on the main dendrite because, looking at the landmark sequences for the period 3 bulb with cusp rays $[\overline{n-1}]$ and $[\overline{n}]$we see the main branching M-point has lateral rays $[(n-1)\overline{n}]$ and $[n(\overline{n-1})]$. The first period doubling rays are likewise $[\overline{(n-1)n}]$ and $[\overline{n(n-1)}]$. Further landmarks noted include the tips and the other main M-point ray. We can

immediately see that the period 4 rays $[\overline{0011}]$ and $[\overline{0100}]$ lie on the largest dendrite beyond the principal M-point.

The M-points can be treated slightly differently. They are all on dendrites, but can be on dendrites of any period, so we need to decode their position sequentially, using the first n-digits to look for ranges in a recursive set of sectors corresponding to the generalized $r^{\infty}$ points, which is made more problematic by the fact that these points have irrational external angles. On the other hand, as noted in fig 13a the addresses of the principal M-points do encode precisely where they are on the tree, so one can alternatively analyse the structure of the eventual periodicity of the M-point to decode its physical address. Looking at these on the period 3 bulb, we see that the principal tip is $[00\bar{1}] = [01\bar{0}]$ which is precisely what we get if we reduce the periodicity of the cusp rays to eventual periodicity 1, the secondary tip is $[\overline{001}]$ which is the eventual period 2 reduction for the lower cusp ray $[\overline{001}]$, and the main branching M-point was analysed above.

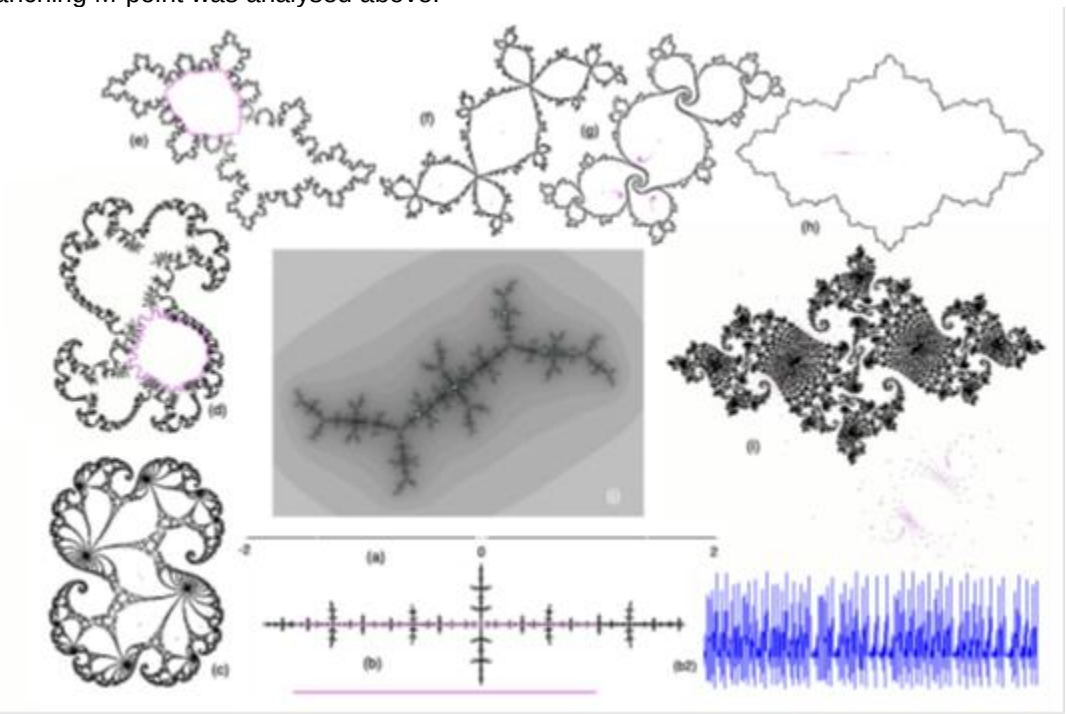

Fig 13b: Julia sets showing (magenta) the varieties of rational and irrational iteration of the critical point. (a) Critical point eventually periodic 0 > -2 > 2 (fixed). (b) Chaotic interval subset of dendritic Julia set (b2) Chaotic dynamics on strange attractor of (b). (c) Neutral points on bulb cusp point, with critical orbit stratified in petals (d,e) Irrational recurrent cycles (Siegel disc) (f) Super-attracting critical point on period 3 (periodic) (g,h) Asymptotically attracting to periods 3 and 1. (i) Seahorse near dendrite with escaping orbit (inset). (j) Fractal strange attractor (cyan) at limit of period doubling on pd 3 bulb. For an image of the collective iteration of all critical points see fig 35. For preimages, and Julia dynamics fig 40, 41.

The variety of dynamics of irrational orbits can better be understood by iterating the critical point and Julia set together. In fig 13b are a variety of periodic and eventually periodic orbits with rational external angles as well as boundary points with recurrent cyclic orbits which are not periodic but densely fill a closed curve, as well as chaotic intervals and fractal strange attractors at the period doubling limit point. The critical point can thus be caught in attracting internal basins, on petals at bifurcation on bulb cusps, be caught in the Julia set itself in chaotic or eventually periodic orbits, and finally can escape to infinity after a sometimes long transient finite orbit near the Julia set. A further dynamic way of viewing the active dynamics in these Julia sets is the wave function method in appendix 1. For a collective image of the iterations of all critical points see fig 35.

### 4. A Heart is only Half a Hamburger: Degenerate Critical Points

A favorite of the standard Mandelbrot function to higher polynomials is to consider simple extensions of the standard function to higher degree i.e. $f(z) = z^d + c$ [4.1]. This certainly gives a one-parameter family of degree $d$ and the results are interesting and beautiful to look at. It is also a trivial extension of deriving the standard cardioid to find the higher dimensional equivalent simply by solving $f(z) = z^d + c = z,\ f'(z) = dz^{d-1} = e^{i\theta}$ together to get $c = z - z^d = d^{-\frac{d}{d-1}}\left( de^{\frac{i\theta}{d-1}} - e^{\frac{di\theta}{d-1}} \right)$ [4.2], which gives a series of dark heart generalizations, to a hamburger, a quartic trefoil of cusps and on to a ($d$–1)-petalled 'polygonal' cusp curve, as shown in fig 14(left). The case for degree 1, as noted in the logistic case, and in all the quadratic bulbs, would be a circle, however the above equation has trivial solution 0 for $d$ = 1.

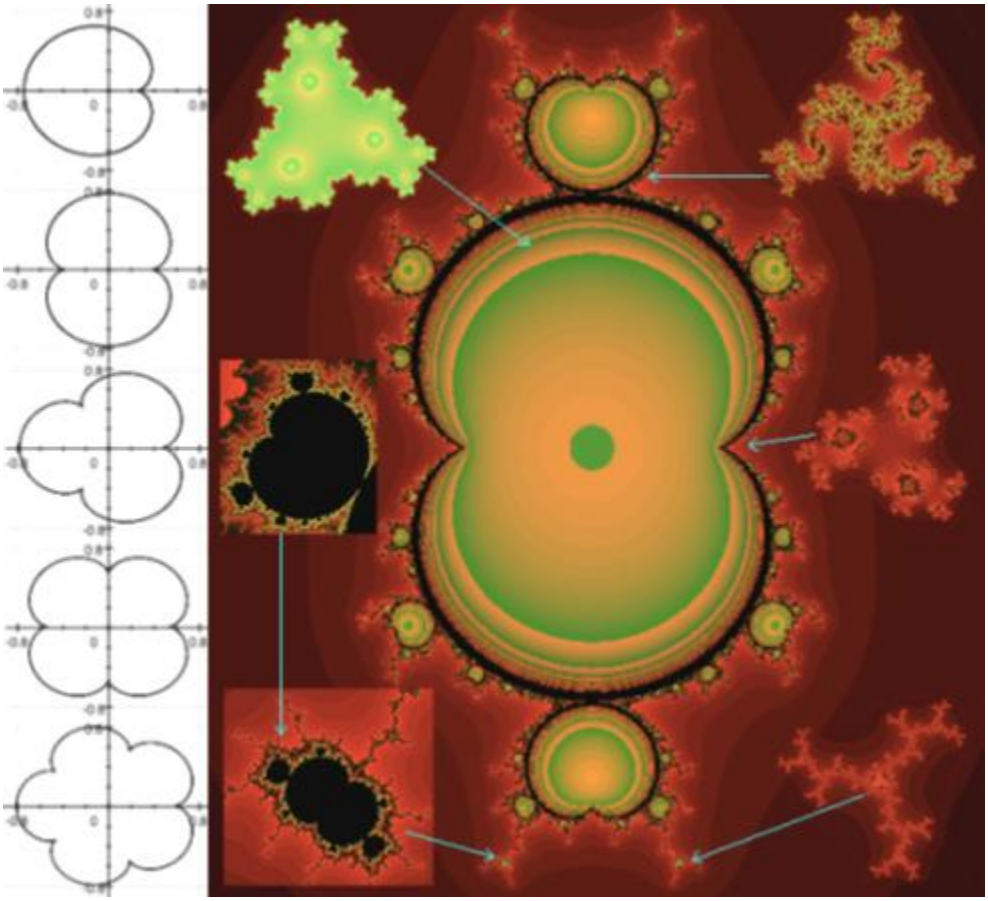

Fig 14: (Right) 'Hamburger Mandelbrot' of $f(z) = z^3 + c$ determines whether the Julia sets are connected or Cantor sets, but these are simply 'triangular' versions of the quadratic sets. Although the main body and all dendritic islands are hamburgers, the bulbs have now all become quadratic 'hearts'. (Left) The series of multi-cusp polygonal curves for higher powers of $z$.

We can see immediately on examining the cubic case in fig 14 that we have a hamburger main body, which is repeated in all dendritic islands, but the bulbs have all now become recursive quadratic hearts. The parameter plane is a defining measure of whether the associated Julia set is connected or a Cantor set, but the Julia sets are simply 'triangular' versions of the same series of Julia sets we saw in the quadratic case. The reason for this is can be seen if we run the process backward by inverse iteration.

We then find $z_n = \sqrt[3]{z_{n+1} - c}$ [4.3] is producing 3 complex cube roots of each point symmetrically arranged around the origin in an equilateral triangle where the quadratic inverse iteration was producing 2.

The reason for this overall profile is that, while the quadratic had a non-degenerate critical point, the single critical point of the higher powers of $z^d + c$ are all degenerate, and in the odd powered case is neither a maximum nor a minimum. The single critical point guarantees the parameter plane does determine the connectivity of the Julia sets because we have only one critical point, but we are missing at least one degree of freedom in the solutions. We thus need to look at more general cubics with non-degenerate critical points.

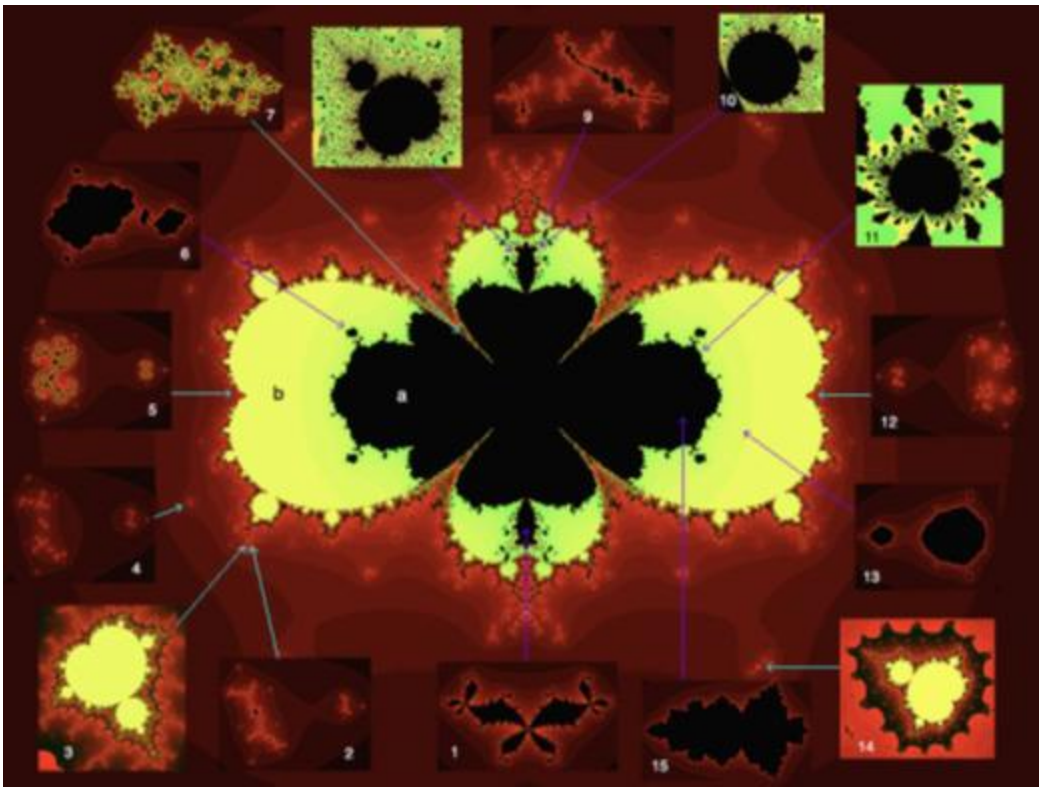


Fig 15: Continuity (a) and Cantor (b) parameter planes of non-degenerate $f(z) = z^3 - z + c$ (a, b) have cardioid dendritic islands (3, 8, 11, 14) and circular bulbs (main figure and 10). Julia sets are Cantor outside both (4, 5, 7, 12) and connected inside both (1, 6, 15). In the yellow region between, we have 1 fractal process connected and one disconnected (2, 9, 13).

**Bibliography:**

1. Barnsley M. (1988) *Fractals Everywhere* Academic Press, New York.
2. Brown D, Halstead M (2007) *Super-attracting cycles for the cosine-root family* Chaos, Solitons and Fractals 31 1191-1202.
3. Dang Y, Kauffman L, Sandin D Hypercomplex *Iterations, Distance Estimation and Higher Dimensional Fractals* http://www.evl.uic.edu/hypercomplex/html/book/book.pdf
4. Devaney R.L. (1986) *An Introduction to Chaotic Dynamical Systems* Benjamin/Cummings, Menlo Park.
5. Douady A, Hubbard J. (1985) *On the dynamics of polynomial-like mappings* Ann Sci Ecole Norm Sup 18, 287-343.
6. Durkin M. (1998) *Observations on the dynamics of the complex cosine-root family* J. Differenc Equat Appl 4 215-28.
7. Epstein A., Yampolsky, M. (1996) *Geometry of the Cubic Connectedness Locus I: Intertwining Surgery* arXivMath/9608213v1

8. Halayka S (2009) Some visually interesting non-standard quaternion fractal sets Chaos, Solitons and Fractals 41 2842–2846
9. Griffin C, Joshi G (1992) Octonionic Julia sets Chaos, Solitons & Fractals 2/1 11-24
10. Griffin C, Joshi G (1993) Transition Points in Octonionic Julia Sets Chaos, Solitons & Fractals 3/1 67-88
11. Hart J C, Sandin D, Kauffman L (1989) *Ray Tracing Deterministic 3-D Fractals* Computer Graphics, 23/ 3 289-296
12. Milnor, John W. (1999). *Dynamics in one complex variable*. Vieweg, Wiesbaden, Germany. ISBN 3-528-13130-6.
13. Pastor G, Romera M, Alvarez G, Montoya F (2002) *Operating with external arguments in the Mandelbrot set antenna* Physica D 171 52–71
14. Romera M, Pastor G, Alvarez G, Montoya F (2006) *External arguments in the multiple-spiral medallions of the Mandelbrot set* Computers & Graphics 30 460-469
15. Peitgen H.O. & Richter P.H., (1986), *The Beauty of Fractals* Springer-Verlag, Berlin. DC
16. Peitgen H.O. et.al. (1988) *The Science of Fractal Images* New York ; Berlin : Springer-Verlag
17. Peitgen H.O., Jurgens H., Saupe D. (2004) *Chaos and Fractals: New Frontiers of Science* New York: Springer.
18. Riemann B (1859) *On the Number of Prime Numbers less than a Given Quantity. http://www.maths.tcd.ie/pub/HistMath/People/Riemann/Zeta/EZeta.pdf*
19. Rochon, D. (2001) *Dynamique bicomplexe et theoreme de Bloch pour fonctions hyperholomorphes*, Doctoral Thesis, Universite de Montreal.
20. Schröder M. (1993) *Fractals, Chaos and Power Laws* ISBN 0-7167-2136-8.
21. Shishikura M. (1994) *The Boundary of the Mandelbrot Set has Hausdorff Dimension Two* Astérisque, 222/7 389-405.
22. Tan Lei (1990) *Similarity between the Mandelbrot set and Julia Sets*, Communications in Math. Phys. 134, 587-617.
23. Woon S (1998) *Fractals of the Julia and Mandelbrot sets of the Riemann Zeta Function* arXiv:chao-dyn/9812031v1

### Internet Links:

MegaPOV http://megapov.inetart.net/download.html
Fractal Domains http://www.fractaldomains.com/download.html
Adobe Pixel Bender http://labs.adobe.com/downloads/pixelbender.html
Tom Beddard's Blog http://www.subblue.com/blog
Mandelbulb Skytopia Site http://www.skytopia.com/project/fractal/mandelbulb.html
Quarternionic Fractal Explorer http://www.theory.org/software/qfe/
3D Fractals Bicomplex Mandelbrot http://www.3dfractals.com/
Buddhabrot Movies http://www.superliminal.com/fractals/bbrot/bbrot.htm
Mu-Ency Mandelbrot Encyclopedia http://www.mrob.com/pub/muency.html